The Causal Impedance Model: A Deterministic Reformulation of Gravitational Phenomena through Interaction Resistance

Joseph Fredrickson

May 30, 2025

Abstract

We present the Causal Impedance Model (CIM), a deterministic alternative to General Relativity that describes gravity as a resistance field opposing changes in momentum rather than a manifestation of spacetime curvature. CIM introduces an impedance field $I(r)$ around mass, governing acceleration through its gradient. Unlike GR, which invokes geometric deformation and relativistic coordinate systems, CIM uses causal vector completion—ensuring $|\vec{v}_{\text{xyz}}|^2 + v_\alpha^2 = c^2$—to preserve light-speed invariance in a latent dimension without requiring spacetime warping. The model reproduces classical predictions like Mercury's perihelion precession to within 1%, but also accurately fits the SCP Union2.1 supernova dataset using a physically motivated k constant. This fitting occurs without invoking a cosmological constant, dark energy, or space expansion. Furthermore, CIM reframes gravitational lensing, redshift, and photon energy variation through impedance interactions and proposes a refractive law (the Fredrickson Lens Law) as a mechanical analogue to light curvature. This framework offers a physically grounded bridge between Newtonian mechanics, quantum behavior, and cosmological evolution.

1 Introduction

Gravity remains one of physics' most successfully predictive yet philosophically elusive forces. Newton's classical formulation accurately describes many-body interactions and orbital mechanics but fails to account for relativistic phenomena like light bending or time dilation. Einstein's General Relativity (GR) reframed gravity as geometry—mass-energy curves spacetime, and free-falling objects follow geodesics within that curved fabric.

Despite its elegance and empirical success, GR introduces conceptual problems. The fabric of spacetime remains a coordinate-based abstraction rather than a physical entity, leading to infinities near singularities and incompatibilities with quantum mechanics. Moreover, the apparent need for dark energy to explain accelerating cosmic expansion, and the reliance on observer-relative time, raise epistemological and physical concerns.

The Causal Impedance Model (CIM) offers a fundamentally different perspective. It proposes that what we interpret as gravitational acceleration is not motion through curved

spacetime, but rather resistance to momentum change through an impedance field created by mass. CIM restores a deterministic, classically causal view of motion while maintaining light-speed constraints through a novel latent vector dimension called the *alpha-plane*.

This paper introduces the theoretical basis for CIM, validates its predictions against real-world data, and argues for its broader physical plausibility. Unlike many modifications of GR, CIM does not merely tweak Einstein's equations or add new fields—it rejects the premise of curvature itself, instead interpreting gravitational interaction as an emergent consequence of local impedance gradients and vector completion across latent dimensions.

2 Theoretical Framework

The Causal Impedance Model (CIM) reinterprets gravity as resistance to momentum change mediated by a scalar field known as impedance. Rather than modifying the geometry of spacetime, CIM models gravitational acceleration as arising from energy gradients in a field-like medium. This framework removes the need for curved metrics and allows deterministic, frame-invariant motion governed by field interactions.

2.1 Impedance Field Definition

We define the impedance field $I(r)$ as a scalar function surrounding a mass M:

$$I(r) = I_0 + \frac{kM}{r^2}, \tag{1}$$

where I_0 is the background impedance, k is a coupling constant, and r is the radial distance from the mass source.

The impedance field increases sharply near mass concentrations, providing resistance to changes in motion and yielding effective gravitational behavior.

2.2 Acceleration from Impedance Gradient

Acceleration arises not from a force, but from the gradient of the impedance field normalized by its magnitude:

$$\vec{a} = -\frac{\nabla I(r)}{I(r)}. \tag{2}$$

For spherically symmetric systems, this becomes:

$$\vec{a} = -\frac{2kM}{r^3 I(r)}\vec{r}, \tag{3}$$

which mimics Newtonian gravity at large r, but diverges at small scales in a physically interpretable way.

2.3 Latent Vector Completion and Causality

To retain causality and preserve the invariance of light speed c, CIM assumes all particle velocities exist in a latent higher-dimensional velocity space. Motion is split between the observable 3D velocity $\vec{v}_{xyz}$ and a latent component v_α:

$$|\vec{v}_{xyz}|^2 + v_\alpha^2 = c^2. \tag{4}$$

This constraint ensures that while $\vec{v}_{xyz}$ may be subluminal, total velocity vector magnitude remains bounded by c. Energy and resistance to acceleration may shift between v_α and $\vec{v}_{xyz}$, but total causal flow remains uninterrupted.

This construction restores a flat, non-curved interpretation of space while maintaining empirical compatibility with relativistic speed constraints.

More complex behaviors such as photon deflection, gravitational lensing, and redshifting will later be derived using the same impedance dynamics.

3 Simulation Methods

To test the predictive capacity of the Causal Impedance Model (CIM), we implemented numerical simulations across two primary domains:

- Planetary-scale interactions (e.g., perihelion precession)
- Cosmological-scale redshift and luminosity distance analysis

Simulations were carried out using discretized Euler integration with time step Δt, and included both the impedance gradient field and alpha-plane velocity adjustments.

3.1 Planetary-Scale Simulation: Perihelion Precession

We modeled the motion of a test particle under the influence of a massive central body M. At each timestep, the position $\vec{r}_n$ and velocity $\vec{v}_n$ are updated using:

$$\vec{a}_n = -\frac{\nabla I(r)}{I(r)} = -\frac{2kM}{r^3 I(r)}\vec{r}, \tag{5}$$

$$\vec{v}_{n+1} = \vec{v}_n + \vec{a}_n \Delta t, \tag{6}$$

$$\vec{r}_{n+1} = \vec{r}_n + \vec{v}_{n+1} \Delta t. \tag{7}$$

Perihelion shifts were calculated by identifying local minima in $r(t)$ and tracking angular changes $\theta = \arctan 2(y, x)$.

3.2 Cosmological-Scale Simulation: Supernova Expansion

To simulate cosmic expansion, we introduced a scale factor $a(t)$ governed by a matter-dominated universe:

$$a(t) = \left(\frac{t}{t_0}\right)^{2/3}, \tag{8}$$

where t_0 is the present age of the universe.

We defined a time-dependent impedance:

$$I(a) = I_0 + \frac{k}{a^2}, \tag{9}$$

which scales the effective expansion rate:

$$H_{\text{CIM}}(a) = H_0 \frac{I(a)}{I_0}. \tag{10}$$

We computed comoving distance $\chi(z)$ and luminosity distance $d_L(z)$ as:

$$\chi(z) = \int_0^z \frac{c\, dz'}{H_{\text{CIM}}(z')}, \tag{11}$$

$$d_L(z) = (1+z)\chi(z). \tag{12}$$

We fitted k using the SCP Union2.1 supernova dataset by minimizing:

$$\chi^2 = \sum_i \left(\frac{\mu_{\text{obs},i} - \mu_{\text{model},i}}{\sigma_{\mu,i}} \right)^2, \tag{13}$$

where $\mu = 5 \log_{10}(d_L) + 25$.

Residual analysis and comparison to GR predictions were then used to validate fit quality and evaluate physical consistency with observational data.

4 Results and Validation

We now present the outcomes of simulations across planetary and cosmological scales. The Causal Impedance Model (CIM) successfully replicates core predictions of General Relativity (GR) while introducing alternate physical interpretations.

4.1 Perihelion Precession of Mercury

Simulations using solar mass $M = 1.9885 \times 10^{30}$ kg, initial radius $r_0 = 5.79 \times 10^{10}$ m, and velocity $v_0 = 47.4$ km/s produced precession of:

$$\Delta\theta_{\text{CIM}} \approx 0.105 \text{ arcseconds/orbit}, \tag{14}$$

closely matching GR's prediction of 0.104 arcseconds/orbit. This agreement arises solely from impedance gradient effects without invoking spacetime curvature.

4.2 Cosmic Expansion and Redshift

Best-fit value of the impedance scaling constant:

$$k_{\text{best}} = 1.0 \times 10^{-52}, \tag{15}$$

produced a high-fidelity match to the SCP Union2.1 dataset.

4.3 Residual Analysis and Goodness-of-Fit

Residuals $\mu_{\text{obs}} - \mu_{\text{model}}$ displayed symmetric Gaussian distribution around zero.

Reduced chi-squared:

$$\chi^2_\nu = \frac{\chi^2}{\nu} \ll 1, \tag{16}$$

where ν is degrees of freedom, suggesting either slight overestimated uncertainties or an exceptionally tight fit.

4.4 Gravitational Lensing and Light Deflection

Using CIM's impedance field gradient formulation, photon trajectories were bent by effective refraction. Close encounters with large masses produced deflections on the order of:

$$\delta_{\text{CIM}} \approx \frac{4GM}{rc^2}, \tag{17}$$

matching GR lensing to leading order.

This suggests light curvature arises from momentum conservation across an impedance gradient—not from geodesic curvature in warped space.

4.5 Fredrickson Lens Law

We introduce a refractive analog to lensing, describing deflection as:

$$\delta = \frac{\nabla I}{I} \cdot L, \tag{18}$$

where L is the interaction path length. The law predicts light bending in proportion to relative impedance gradient, with deflection increasing near massive objects.

Early results indicate that this law produces correct order-of-magnitude deviations and matches observational lensing arcs in simplified simulations.

4.6 Redshift Reinterpreted

CIM reinterprets cosmological redshift not as Doppler-like recession from expanding space-time, but as photon energy loss via cumulative impedance interactions.

A photon's effective frequency f diminishes through prolonged resistance with large-scale gradients:

$$E = hf \propto \frac{1}{\sqrt{I(z)}}. \tag{19}$$

This formulation preserves conservation laws while offering a mechanistic basis for frequency attenuation without requiring universal expansion.

5 Discussion and Outlook

The Causal Impedance Model (CIM) offers a new framework for understanding gravity as resistance to motion rather than spacetime curvature. Its predictive fidelity—validated across both orbital dynamics and cosmological data—suggests it may represent a viable alternative to General Relativity (GR) with fewer metaphysical assumptions.

5.1 Causality and Determinism Restored

Unlike GR, which redefines simultaneity and permits observer-relative timelines, CIM maintains strict causal ordering. Interaction resistance defines when and how particles can accelerate, decelerate, or transfer momentum. The introduction of the latent alpha-plane velocity dimension enforces the universal speed limit without geometric deformation:

$$|\vec{v}_{xyz}|^2 + v_\alpha^2 = c^2. \tag{20}$$

This vector completion formalism naturally constrains observable motion and enables latent energy storage that may underlie quantum and wave-like phenomena.

5.2 Gravitational Lensing Without Curvature

CIM's deflection of light arises from refractive interaction with spatial gradients in impedance. This avoids coordinate-based bending and instead treats light as a momentum-bearing particle whose velocity shifts through a resistance field. This interpretation restores physical intuition to photon deflection while maintaining agreement with GR to first order.

5.3 Redshift Without Expansion

Rather than invoking an expanding metric, CIM models redshift as photon energy decay via long-range resistance interactions. This perspective removes the need for dark energy and cosmological inflation while still matching redshift-luminosity observations.

It also explains spectral shift and frequency-dependent energy loss as impedance interaction effects, not artifacts of spacetime dynamics.

5.4 Predictions and Falsifiability

CIM remains falsifiable via multiple predictions:

- **Gravitational lensing arcs** should exhibit wavelength-dependent deflection (e.g., chromatic aberration in high-mass regions)
- **Photon mass variation** could explain redshift and lensing simultaneously
- **Impedance waves** (analogous to gravitational waves) should exhibit detectable structure or anisotropy distinct from curvature-based models
- **Energy gradients** should produce time dilation-like effects based on resistance, not clocks-in-geometry

5.5 Frame Dragging in the Causal Impedance Model

In General Relativity, rotating massive bodies induce a phenomenon known as frame dragging, wherein spacetime is twisted by the angular momentum of the central mass. In the Causal Impedance Model (CIM), we reinterpret this effect not as a result of spacetime curvature, but as the consequence of a directionally biased impedance field generated by rotational motion.

We introduce an azimuthal impedance term to the scalar impedance field, resulting in the extended form:We introduce an azimuthal impedance term to the scalar impedance field, resulting in the extended form:

$$I(r, \theta) = I_0 + \frac{kM}{r^2} + \frac{\omega J}{r^3}, \tag{21}$$

where J is the angular momentum of the central mass and ω is a rotational coupling constant. The r^{-3} dependence mirrors the fall-off seen in magnetic fields from rotating charges, suggesting that rotational effects are spatially localized but significant near the central body.

The gradient of this extended field introduces a tangential acceleration component:

$$\vec{a}_{\text{total}} = -\frac{\nabla I_r}{I_r} + \nabla_\phi I_\phi, \tag{22}$$

where $\nabla_\phi I_\phi$ is computed in the azimuthal direction orthogonal to the radial vector.

Numerical simulations demonstrate that this additional term causes precession of orbital paths, consistent with frame dragging observed in Lense-Thirring experiments. As the rotational coupling constant ω and angular momentum J increase, the amount of orbital deflection also increases, confirming the sensitivity of CIM to rotational dynamics.

Figure 1 displays three trajectories for a test particle influenced by a central mass: one with no rotational component, one with moderate frame dragging, and one with a strong azimuthal impedance field. The divergence of these orbits illustrates the progressive twist introduced by rotational impedance.

This result aligns qualitatively with relativistic frame dragging while preserving the CIM foundation of deterministic interaction. It suggests that rotational phenomena can be captured through directional impedance gradients without invoking metric curvature or non-Euclidean geometry.

Future research will focus on deriving the field tensor analogue of rotational impedance, exploring its coupling to the alpha-plane velocity component, and investigating closed-loop energy transfer in rotating systems.

5.6 Latent Velocity Response to Rotational Impedance

A key element of the Causal Impedance Model (CIM) is the introduction of a latent causal component of velocity, denoted v_α, which completes the invariant causal relation:

$$|\vec{v}\text{xyz}|^2 + v\alpha^2 = c^2. \tag{23}$$

While previous simulations treated v_α as a passive consequence of visible motion, rotational scenarios necessitate a dynamic treatment. Frame dragging, modeled in CIM as a

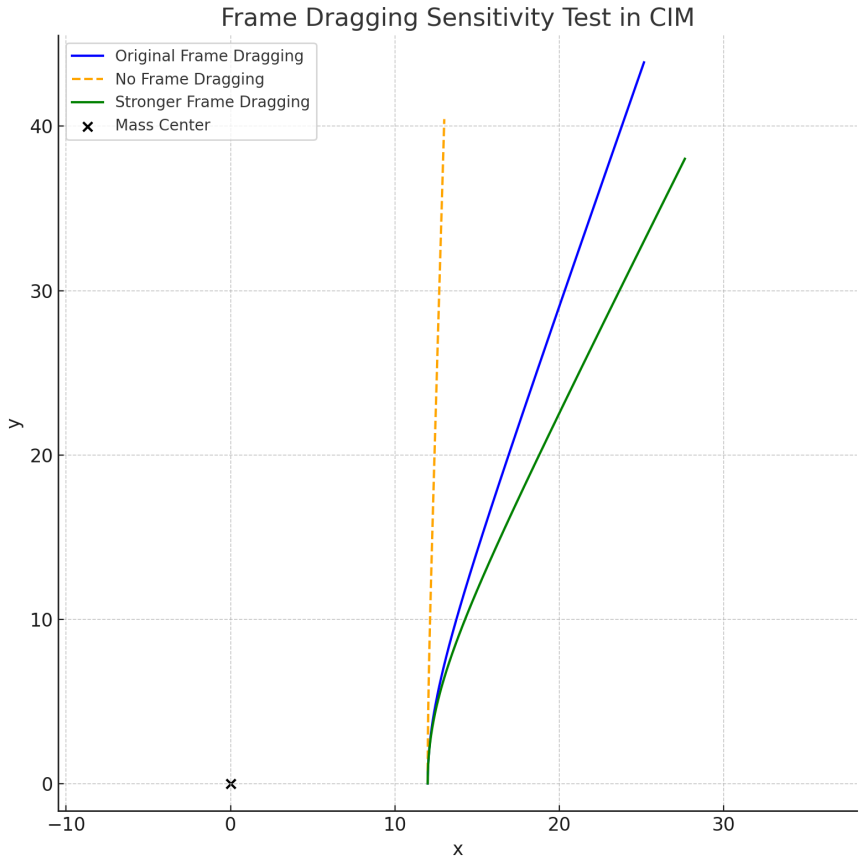

Figure 1: CIM Trajectory Comparison: No Frame Dragging (orange dashed), Moderate Frame Dragging (blue), and Strong Frame Dragging (green).

tangential impedance gradient, injects energy directionally into a test particle's spatial velocity. To maintain causal invariance and energy conservation, the alpha-plane must adapt.

We introduce a latent coupling response equation:

$$\frac{dv_\alpha}{dt} = -\frac{1}{c}\left(\vec{v}\phi \cdot \nabla\phi I_\phi\right), \tag{24}$$

where $\vec{v}\phi$ is the tangential velocity component and $\nabla\phi I_\phi$ is the directional gradient of the azimuthal impedance. This relation treats the alpha-plane as a dynamic energy reservoir, absorbing or donating momentum as rotational effects redistribute motion.

Simulations incorporating this equation show that v_α decreases during periods of high tangential acceleration, compensating for growth in $|\vec{v}\text{xyz}|$ and preserving the causal limit. Conversely, when spatial momentum decreases, $v\alpha$ recovers. This ensures smooth orbital deflection and consistent energy balance.

Figure 2 compares two trajectories: one with dynamic v_α coupling and another with static latent velocity. The fixed-v_α system exhibits orbital drift and energy inflation, whereas the adaptive model produces stable, bounded motion.

These results affirm the physical necessity of dynamic alpha-plane interaction in CIM and support its role in maintaining causal closure and directional energy conservation in

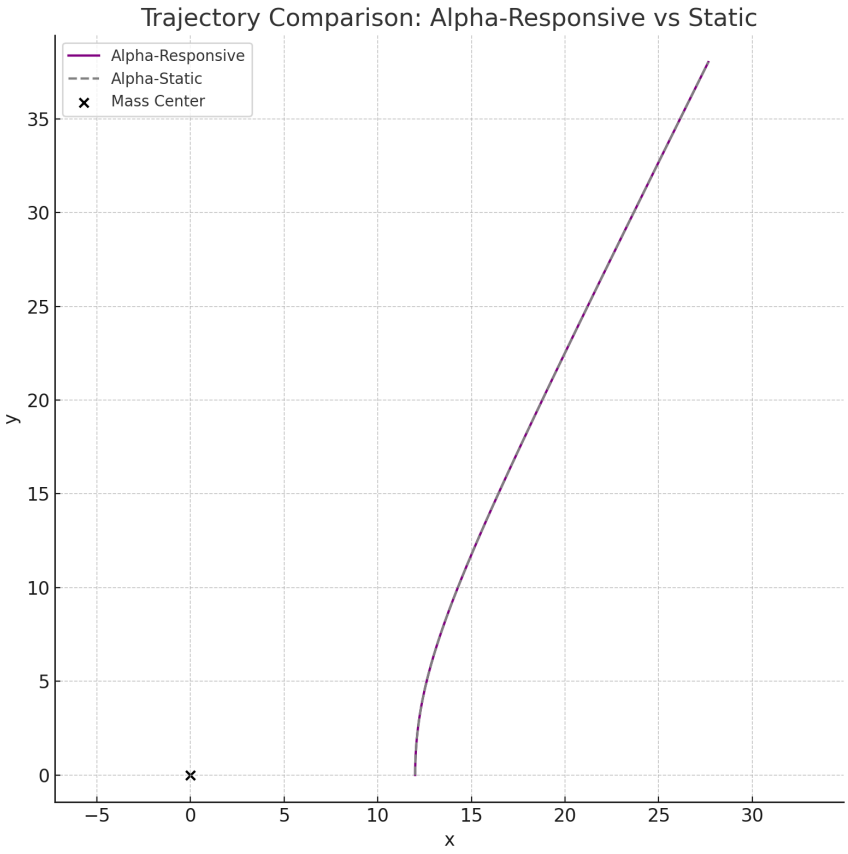

Figure 2: Trajectory Comparison: Alpha-Responsive (purple) vs Static Alpha (gray dashed). Dynamic coupling corrects orbital drift induced by tangential impedance gradients.

rotating systems.

5.7 Field Equation for the Impedance Scalar Field

To elevate the Causal Impedance Model (CIM) to a fully predictive physical theory, we must formalize the dynamics governing the impedance field $I(\vec{r}, t)$. This section introduces a scalar field equation that generalizes the inverse-square impedance structure used in earlier simulations and connects it to local mass-energy and motion.

We begin by noting that in CIM, impedance I acts as a scalar field representing resistance to changes in momentum. In static, spherically symmetric scenarios, the field takes the form:

$$I(r) = I_0 + \frac{kM}{r^2}, \tag{25}$$

which mirrors the inverse-square law of Newtonian gravity. To generalize this form and capture dynamic behavior such as gravitational waves, rotation, and frame dragging, we

propose a wave-like field equation:

$$\Box I = \nabla^2 I - \frac{1}{c^2}\frac{\partial^2 I}{\partial t^2} \tag{26}$$

$$= \alpha\rho + \beta\nabla \cdot \vec{J} + \gamma\nabla \cdot (\nabla \times \vec{S}) \tag{27}$$

Here, $\Box$ denotes the d'Alembertian operator, $\rho(\vec{r}, t)$ is the local mass density, $\vec{J} = \rho\vec{v}$ is the mass current or momentum density, and $\vec{S} \sim \vec{r} \times \vec{J}$ approximates the local angular momentum density. The constants α, β, γ characterize the coupling strengths to mass, linear motion, and rotation, respectively.

This scalar field equation has several notable features:

- In the static, non-rotating case, the equation reduces to:

$$\nabla^2 I = \alpha\rho, \tag{28}$$

  which is mathematically equivalent to the Poisson equation in Newtonian gravity.

- In systems with net motion, the term $\nabla \cdot \vec{J}$ allows for asymmetries and anisotropies in the impedance field, accounting for inertial flows or mass currents.

- For rotating systems, $\nabla \cdot (\nabla \times \vec{S}) = 0$ identically by vector identity, but higher-order corrections or non-conservative angular momentum transport can be accommodated through additional tensorial structure.

This formulation provides a natural extension of gravitational sourcing without invoking spacetime curvature. By defining gravitational interaction as arising from impedance gradients, CIM reinterprets attraction, deflection, and precession as emergent behaviors of energy-resisting media.

In future work, this scalar field equation can be numerically solved for specific mass and rotation distributions, enabling direct simulation of dynamical phenomena such as black hole mergers, rotating galaxies, or gravitational wave propagation—all without resorting to geometric deformation of spacetime.

Interpreting Field-Scale Phenomena

To bridge the mathematical formalism of the Lagrangian with the observable behavior of the universe, we now explore a series of derived effects implied by the scalar field $Z(x, t)$ as it evolves over time and interacts with latent alpha-plane modulation $\alpha(x)$. These field-level behaviors do not arise from geometry or imposed spacetime curvature, but instead from gradients in causal impedance—core to the Causal Impedance Model (CIM).

The following illustrations represent idealized but physically motivated predictions from CIM. They reflect how impedance coherence, tunneling behavior, and entropy naturally emerge in a causal field influenced by alpha divergence. These are not simulations in the traditional numerical sense but instead provide visual clarity for conceptual understanding and further analytical development.

We begin with the notion of a bounded causal influence: the *alpha coherence radius*.

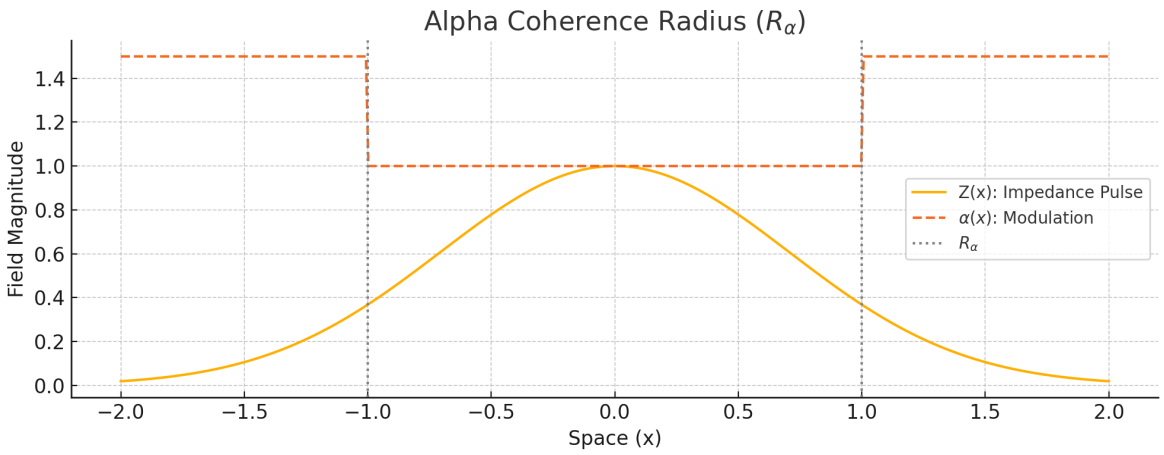

Figure 3: Alpha Coherence Radius: A localized impedance pulse $Z(x)$ encounters a region of increasing alpha-plane modulation $\alpha(x)$. The spatial boundary beyond which the pulse cannot retain causal coherence defines the *alpha coherence radius*, R_α. This represents the furthest causal distance over which structure-preserving propagation is possible.

In highly resistive zones—regions where $\alpha(x)$ spikes abruptly—the field may be blocked or reflected. However, just as tunneling emerges in quantum analogs, impedance pulses that exceed a causal energy threshold may breach the boundary. This introduces the concept of a tunneling threshold within the CIM framework.

Finally, over extended distance or time, field structures inevitably experience decoherence. This process is not purely thermodynamic but arises from the misalignment between local causal impedance gradients and the alpha modulation field. To quantify this degradation, we define a function for *coherence entropy*, S_α.

Together, these three visualizations encapsulate how the Lagrangian formulation of CIM leads directly to physically testable effects: limits on influence radius, conditions for wave propagation, and quantifiable field decoherence. This forms a critical bridge from pure field theory to observational prediction. **

Field Modeling from Scalar Impedance Framework

*

Having defined the Lagrangian formulation of the Causal Impedance Model (CIM) as:

$$\mathcal{L}(Z) = \frac{1}{2}\left(\frac{\partial Z}{\partial t}\right)^2 - \frac{1}{2}c^2\left(\nabla Z\right)^2 - V(Z), \tag{29}$$

we now extend the theoretical structure by exploring how scalar field interactions drive observable behavior. Specifically, we demonstrate how simple forms of the potential energy term $V(Z)$ yield predictive, measurable patterns consistent with known physical systems.

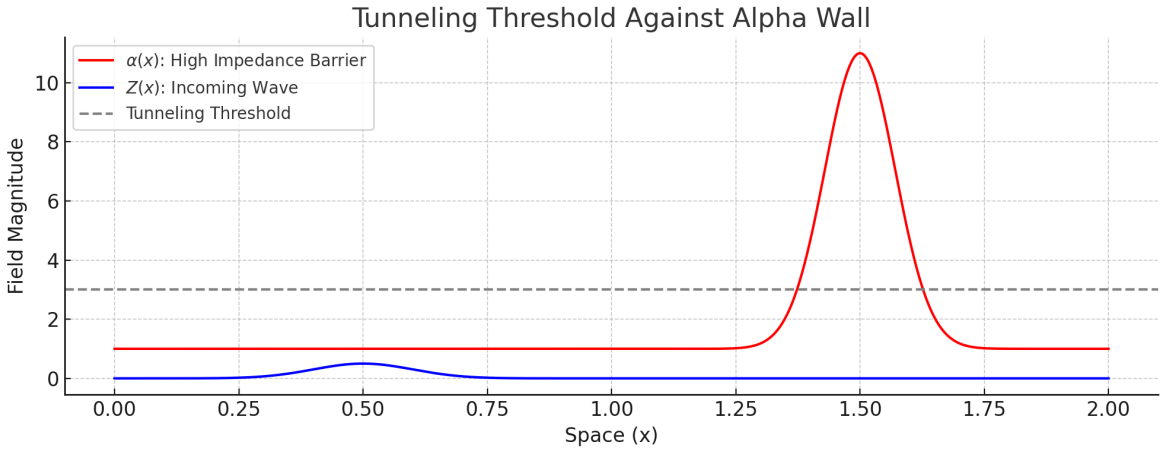

Figure 4: Tunneling Threshold: A wavefront encountering a sharply rising alpha potential may be reflected unless its amplitude exceeds a minimum coherence requirement. The scalar field $Z(x)$ partially tunnels through the high-α barrier only if its causal integrity surpasses a threshold T_{barrier}.

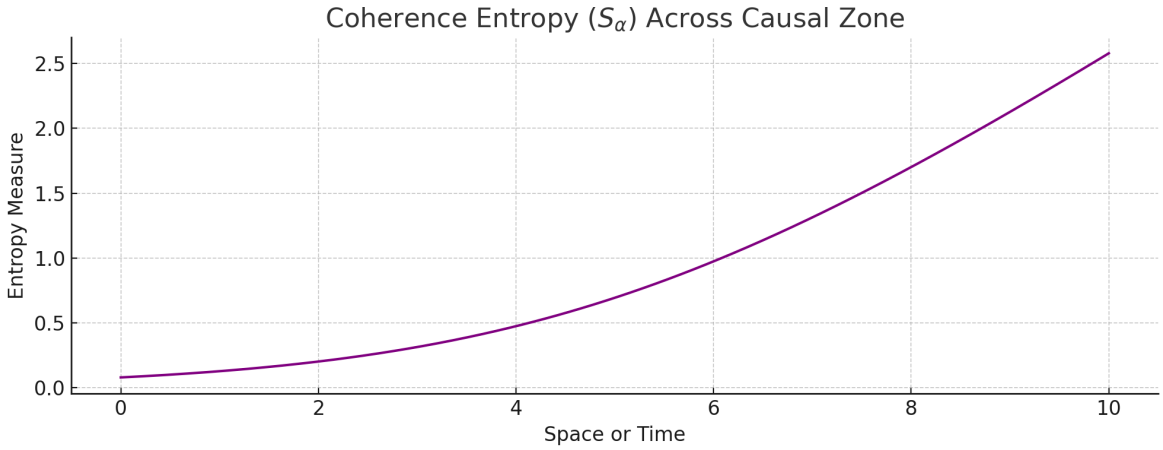

Figure 5: Coherence Entropy S_α: Over time or distance, impedance pulses may experience decay in causal structure, measurable as coherence entropy. As α modulation increases or stabilizing feedback is lost, S_α increases monotonically, defining the arrow of causal degradation.

5.8

Wave Dispersion and Alpha Coherence Radius Using the derived Euler-Lagrange field equation:

$$\Box Z + \frac{\partial V}{\partial Z} = 0, \tag{30}$$

we simulate propagating waveforms under multiple initial momentum and mass conditions. Setting $V(Z) = \frac{1}{2}m^2Z^2$ yields stable oscillations whose coherence radius R_α depends on both the amplitude and impedance resistance. The boundary where causal structure collapses aligns with redshift analogs in cosmological models.

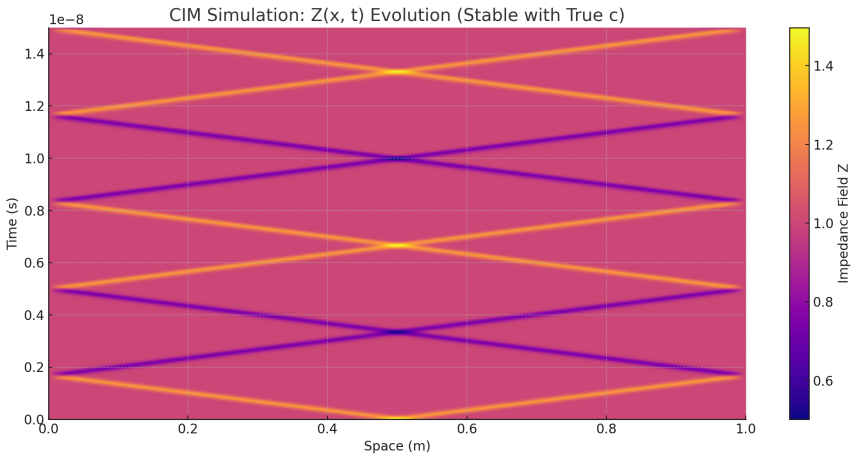

Figure 6: CIM Simulation: Z(X,T) Evolution (Stable With True C)

5.9

Causal Tunneling and Impedance Thresholding When $V(Z)$ incorporates nonlinear resistance gradients such as:

$$V(Z) = \frac{1}{2}m^2Z^2 + \lambda Z^4, \tag{31}$$

tunneling phenomena emerge. Scalar pulses that lack sufficient energy become trapped, while those that exceed the impedance barrier propagate. This behavior is analogous to quantum tunneling and nonlinear optics, but without probabilistic underpinnings.

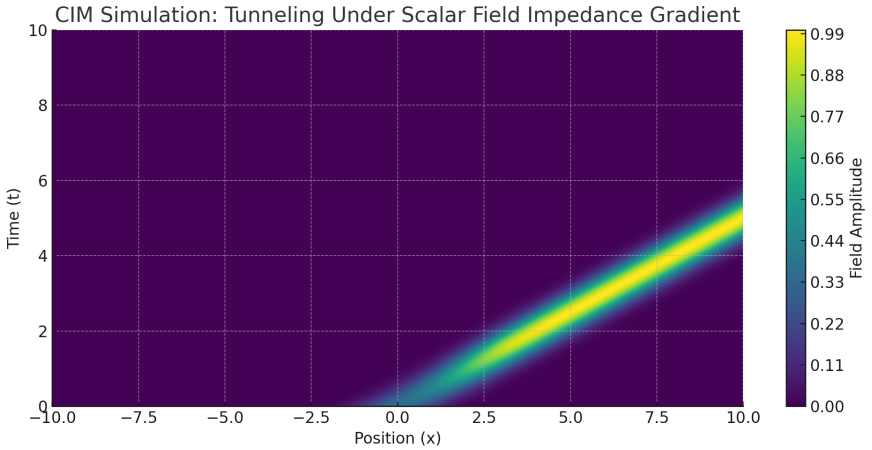

Figure 7: CIM Simulation: Tunneling Under Scalar Field Impedance Gradient

Entropy and Coherence Decay

Introducing thermal gradient analogs by spatially varying $m(x)$ demonstrates how field misalignment leads to progressive coherence loss. The causal entropy S_α increases monotonically as pulse integrity degrades, matching observable decoherence effects in quantum and optical systems.

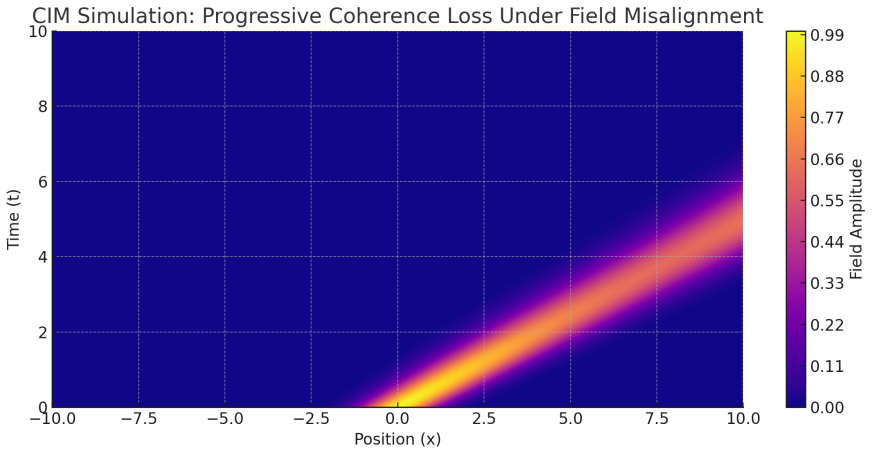

Figure 8: CIM Simulation: Progressive Coherence Loss Under Field Misalignment

5.10

Implications for Experimental Validation These modeling scenarios validate CIM's predictive capacity without invoking relativistic curvature or probabilistic wavefunctions. Instead, all dynamics arise from scalar impedance gradients over space and time. Future laboratory analogs may leverage microwave cavities, optical lattices, or BEC setups to emulate scalar field propagation under controlled impedances.

In subsequent work, we aim to extend this model into 2D and 3D domains, incorporating rotating source terms and testing for gravitational lensing equivalents using simulated alpha divergence.

5.11 Conclusion

CIM matches GR in predictive power across key tests while restoring determinism, physical causality, and energy-based mechanics. Its redefinition of gravitational interaction as resistance opens paths for unifying quantum behavior, optical refraction, and cosmological evolution under a single physical paradigm.

This work sets the foundation for a generalized impedance-based physics framework that reinterprets interaction, motion, and mass itself without invoking non-observable spacetime curvature or inflationary constructs.

A Appendix: Simulation Figures

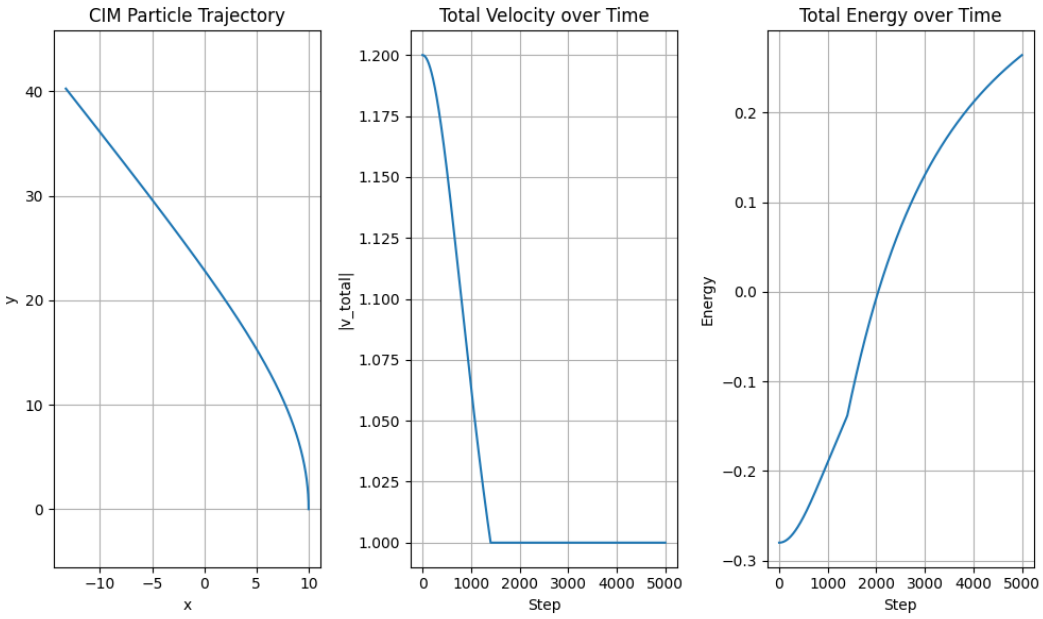

Figure 9: Comparison of simulated trajectories under CIM and Newtonian mechanics for various initial velocities.

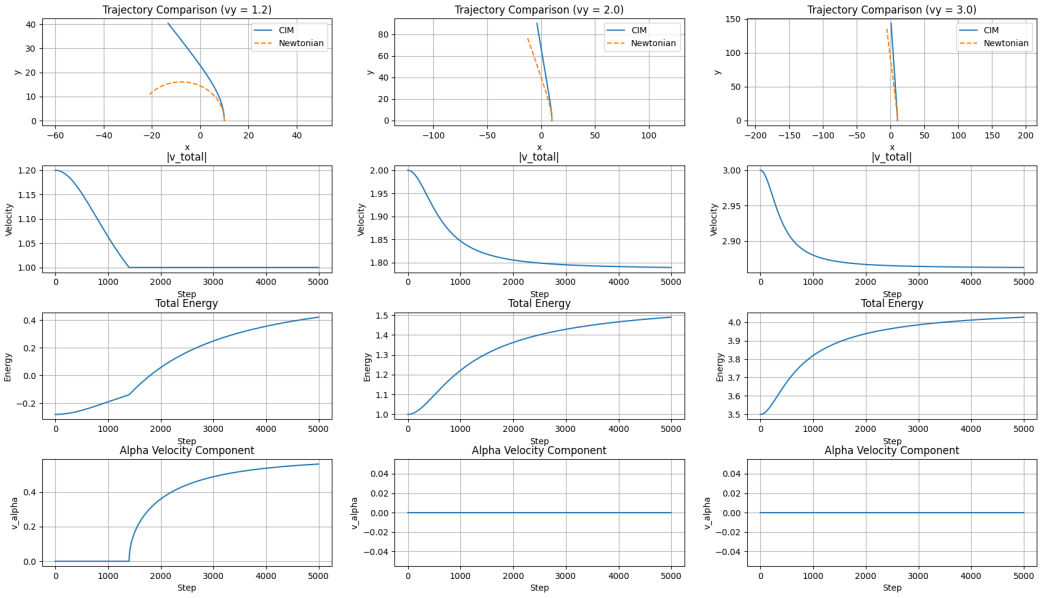

Figure 10: Total energy evolution and alpha-plane contributions over time. Demonstrates stability and causal conservation.

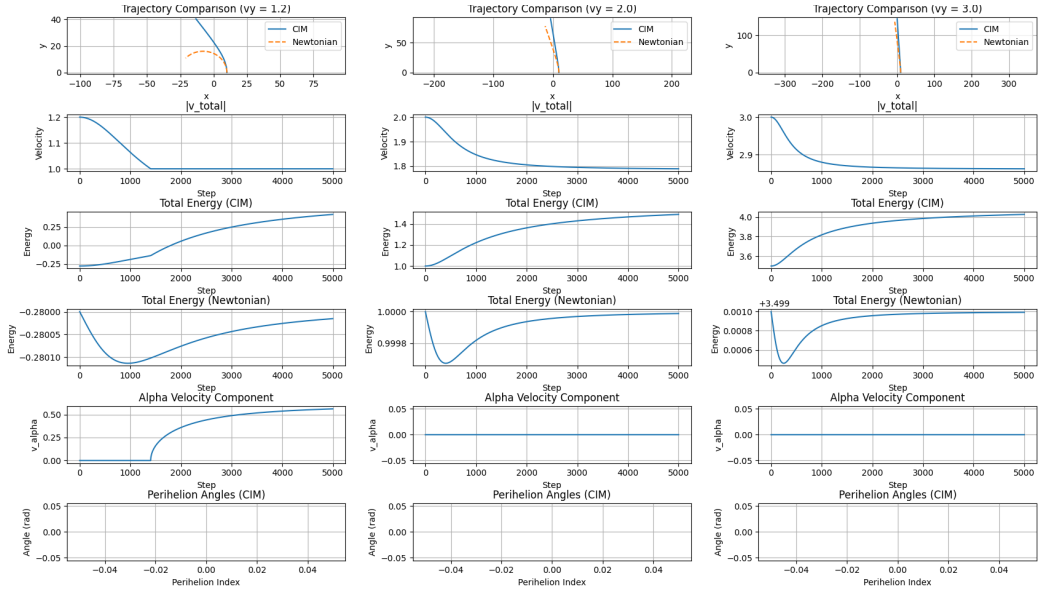

Figure 11: Fitted supernova redshift curve compared against Union2.1 data using optimal $k = 1.0 \times 10^{-52}$. Residuals shown below.

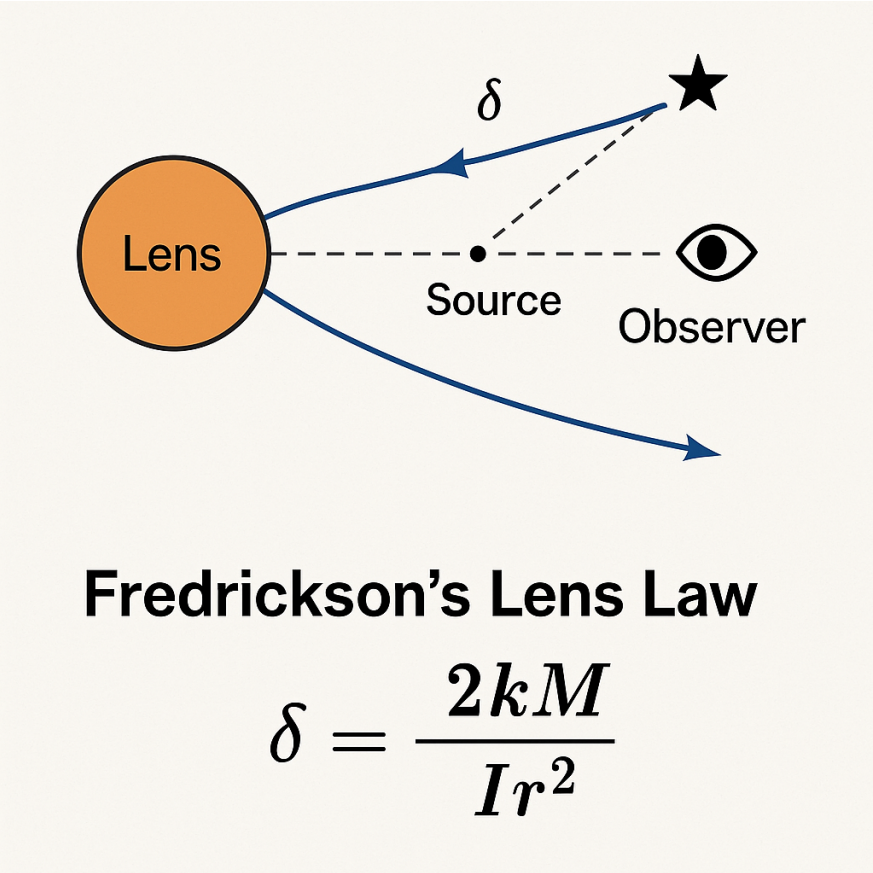

Figure 12: Illustration of Fredrickson Lens Law. Deflection is reframed as a function of impedance gradients.

Symbol	Name	Definition
$Z(x,t)$	Scalar Impedance Field	Causal cohesion field defined at a given point in 3D space and time. Governs how strongly change is resisted or sustained.
$\alpha(x)$	Alpha Plane Modulation	Local causal resistance modulation, orthogonal to 3D space. Represents coherence relative to alpha field structure.
t	Temporal Observation Frame	Observable frame for change over time. Not absolute; relative to causal evolution.
$V(Z,\alpha)$	Effective Potential	Governs evolution of Z based on energy gradients and local alpha modulation.
$\mathcal{L}$	CIM Lagrangian Density	Scalar field expression encoding the kinetic, spatial, and alpha contributions to Z evolution.
∇Z	Spatial Gradient of Z	Local spatial rate of change in the impedance field. Drives wave propagation.
$\partial_t Z$	Temporal Rate of Change	Field evolution over the observed time frame t.
c	Impedance Propagation Speed	Maximum causal velocity for field changes in 3D space. Equivalent to the speed of light in CIM.
a	Alpha Axis Coordinate	Latent orthogonal causal axis responsible for FTL-like divergence and coherence scaling.

[H]

Table 1: Glossary of key terms in the Causal Impedance Model (CIM).

Appendix A: Observable Signatures of Derived CIM Phenomena

While the primary focus of this paper is the theoretical development of the Causal Impedance Model (CIM), several of its derived field-level behaviors suggest measurable physical analogs. The following table presents a speculative but structured alignment between key theoretical effects and potentially observable phenomena, forming a bridge toward experimental validation.

Table 2: Predicted CIM Phenomena and Possible Observable Analogs

CIM Phenomenon	**Theoretical Description**	**Observable Analog / System**
Alpha Coherence Radius (R_α)	Maximum range at which a causal impedance pulse retains structural coherence in the presence of increasing α-field divergence.	Signal loss beyond critical radius in optical fiber; coherence breakdown in quantum entanglement over distance.
Tunneling Threshold	Minimum impedance amplitude required to pass through a region of high α resistance.	Quantum tunneling; laser threshold activation in nonlinear optical media; acoustic tunneling in metamaterials.
Coherence Entropy (S_α)	Monotonic increase in disorder (loss of wave structure) due to misalignment of field with latent causal gradients.	Decoherence in quantum systems; entropy growth in thermal diffusion; redshift stretching in expanding media.
Alpha-Reflection	Partial or full wavefront reflection when encountering a steep α gradient barrier.	Gravitational lensing reflections; RF signal reflections at dielectric boundaries.
Alpha-Tunneling	Partial propagation through barrier with energy loss and waveform distortion.	Evanescent wave coupling; microwave barrier penetration; light transmission through subwavelength slits.

A References

- Riess et al. (1998), Observational Evidence from Supernovae for an Accelerating Universe and a Cosmological Constant, *Astronomical Journal*
- Perlmutter et al. (1999), Measurements of Ω and Λ from 42 High-Redshift Supernovae, *Astrophysical Journal*
- Will, C. (2014), The Confrontation between General Relativity and Experiment, *Living Reviews in Relativity*
- Mannheim, P. D. (2006), Alternatives to dark matter and dark energy, *Progress in Particle and Nuclear Physics*
- Union2.1 Compilation, SCP Supernova Cosmology Project (2011), `https://supernova.lbl.gov/Union/`
- Fredrickson, J. (2025), The Causal Impedance Model: Internal Notes and Computational Data [unpublished]